Korean J. Chem. Eng., 33(3), 775-781 (2016)
DOI: 10.1007/s11814-015-0197-5

pISSN: 0256-1115
eISSN: 1975-7220

New criteria for filament breakup in droplet-on-demand inkjet printing using volume of fluid (VOF) method

Sadegh Poozesh†, Nelson Akafuah, and Kozo Saito

IR4TD, Mechanical Engineering Department, University of Kentucky, Lexington, KY 40506, U.S.A.
(*Received 22 May 2015 • accepted 16 September 2015*)

Abstract−A volume of fluid (VOF) numerical study is presented in which new pi number-based criteria are discussed that identify and separate three different regimes for a droplet-on-demand (DOD) print-head system. A trailing filament coalesces into the main droplet while the filament breaks into one or multiple satellite droplet(s). The numerical simulation results are compared with published large-scale experimental results that used a 2 mm diameter inkjet nozzle head, roughly 50 times larger than the actual diameter of inkjet outlets. Liquid filament break-up behavior is predicted using a combination of two pi-numbers, including either *Weber (We)-Ohnesorge (Oh)* number couplets or *Reynolds (Re)-Weber (We)* number couplets that are dependent only on the ejected liquid properties and the velocity waveform at the print-head inlet. These new criteria have merit over the currently existing ones that require accurate measurements of actual droplets to determine filament physical features like length and diameter [1].

Keywords: Inkjet Printing, Droplet on Demand, Scale Modelling, Volume of Fluid (VOF), Filament Breakup

INTRODUCTION

Inkjet printing recreates digital images by producing and transporting tiny (10-100 μm) ink droplets to surfaces to be printed. Inkjet printing has moved beyond just a computer printing process and has become a versatile technology having important benefits in material coating, electronic circuits, drug delivery, printing of electronics and biomaterials, DNA arranging, fabricating micro-electro-mechanical systems (MEMS) components, manufacturing of particles and microcapsules, and spraying processes [2-6]. Although a large range of inkjet technologies exist, two dominant contemporary industrial applications are continuous inkjet (CIJ) and drop-on-demand (DOD). The former uses pressure modulation to break a liquid stream into well-controlled droplets, while the latter uses piezoelectric elements or thermal heaters to create discrete pressure pulses that break a liquid stream.

This study focuses on DOD and examines two issues of importance for inkjet technologies: reducing droplet size and satellite droplets [7]. Previous studies [7,8] have revealed that the radii of generated droplets are nearly the same as the radius of nozzle from which the droplets emanate. For high precision applications, where droplet radii of 2 μm or less are required, the nozzle radius also has to be near 2 μm; hence, the nozzles become susceptible to plugging or breaking [8]. Therefore, research has been performed on how to decrease droplet size without reducing nozzle size [7,8]. Results in the current study also confirm that the main droplet size is approximately the same as the nozzle size; however, the focus here would be only on eliminating satellite droplet issue.

Dong et al. [9], in an experimental study on the dynamics of DOD droplet formation while employing a piezo-electrical actuated inkjet print-head with a wide range of liquid viscosities and surface tensions, examined effects of the print head driving signal, and liquid properties and behaviors, including the ejection and stretching of the liquid, thread pinching at the nozzle exit, liquid thread contraction, liquid thread breakup into a primary drop and satellites, and the recombination of the primary droplets with satellites. They were able to show that after pinching off and during contraction of the liquid filament, two modes of breakup could be observed, one of which was associated with end-pinching where the liquid thread pinched off from an almost spherical head and the other of which was multiple breakup. The effects of the liquid and system parameters on these two modes and satellite formation mechanisms were examined in detail.

Castrejon-Pita et al. [10], based on experimental data from a liquid jet generator capable of producing free cylindrical liquid filaments, discussed the conditions under which a liquid filament would break into drops with a focus on a wide range of two dimensionless quantities: the aspect ratio of the filament, i.e. the filament length-divided by-its diameter, and the Ohnesorge (Oh) number.

After ignoring the motion of the massive print head relative to the tail, Hoath et al. [1] predicted the behavior of an asymmetric, single-ended filament of length l attached to a large drop by assuming it was equal to free cylindrical filaments studied by Castrejón-Pita et al. [10], but with a length twice that as the single-ended one; these types of asymmetric, single-ended filaments have been observed to occur in inkjet droplets. As a consequence, using print-head drive waveforms that produced liquid jets with only a small initial relative, lateral speed between the two ends of the filament a critical transition region above which the ejected liquid filament broke into more than one droplet.

Computational fluid dynamics (CFD) studies [11-15] have also been accomplished that have assessed the dynamics of filament

†To whom correspondence should be addressed.
E-mail: sadegh.poozesh@gmail.com

breakup. Fromm's pioneering numerical simulation study [12] used a marker-and-cell (MAC) method to analyze axisymmetric dynamics of drop formation from a DOD nozzle. More recently, Xu and Basaran [14] applied the method of lines coupled with a Galerkin finite element method model for spatial discretization and an adaptive finite difference method for time integration to solve transient equations for an incompressible Newtonian fluid from a simple capillary tube. Imposing a time-periodic inflow rate, they described a regimen map with three regions that had three modes of breakup based on *We*, *Oh*, droplet size parameter and the inlet flow rate frequency.

Castrejon-Pita et al. [11] designed a large scale 2 mm diameter nozzle attached to a generic commercial DOD print-head nozzle of 50 μm diameter which was operated with a droplet speed 6 m/s; they visualized droplet shapes using a shadow-graph technique. The primary similarity jetting parameters were identified as Oh and We and then kept them constant during large-scale model experiments and generic commercial nozzle operation. They also modeled the operation using the Lagrangian finite-element method with Oh and We scaling parameters while neglecting gravity; their results showed agreement between the modeling and experimental results. Employing numerical simulation based on volume of fluid (VOF) model, Kim and Baek [13] obtained a printability map that described different liquid filament breakup mechanisms based on Oh, We, and capillary (Ca) non-dimensional parameters.

Based on an assessment of the aforementioned studies, Fig. 1 was created to depict two different modes of droplet breakup: (a) a liquid thread ejected from the nozzle contracts into a single drop without breaking up; and (b) a liquid thread ejected from the nozzle breaks up to form two or more independent droplets. For optimal operation during inkjet printing, mode (a) is favored whereas mode (b) is not. The reasons for a transition between modes (a) and (b) are not well-understood; hence, this research attempts to provide insight into the dynamics of the transition between these two different modes.

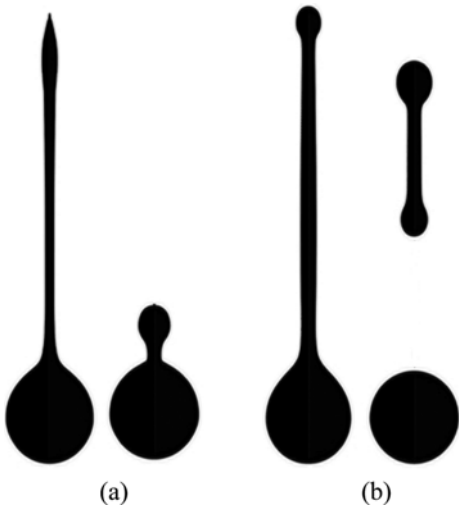

Fig. 1. Two modes of the second breakup: (a) Single droplet formation where the liquid thread (left) forms an almost spherical droplet (right) without breakup, and (b) the liquid thread (left) creates a spherical droplet and a separate liquid thread (right).

PROBLEM STATEMENT

As a basis for the current study, the type of physical system used

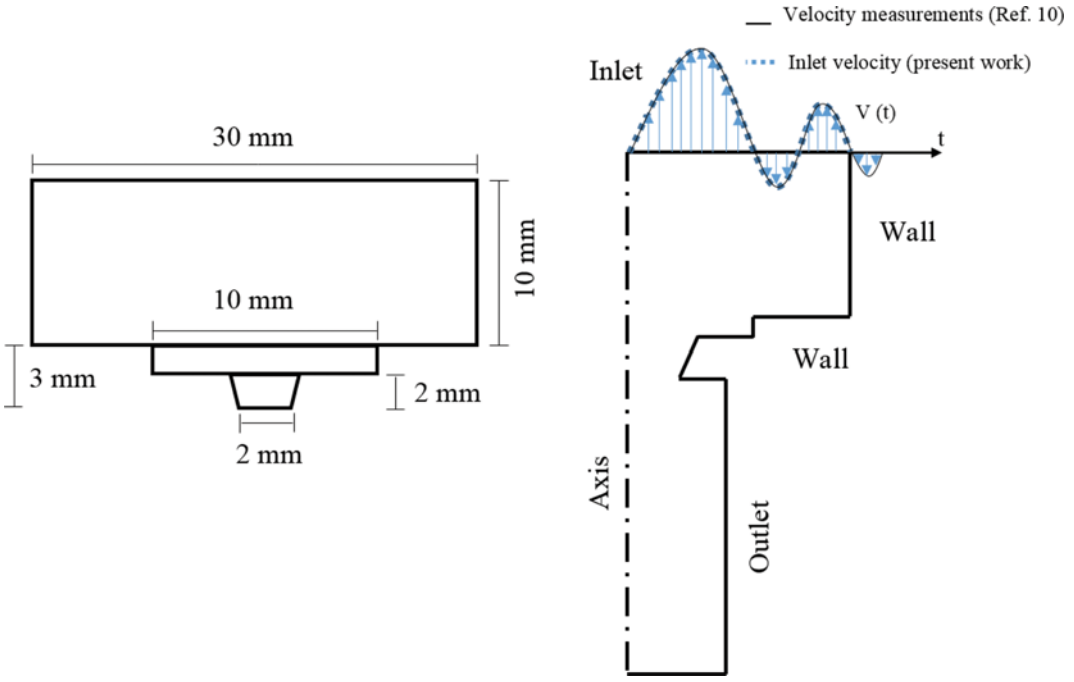

Fig. 2. Schematic of the a large scale (nozzle diameter: 2 mm) inkjet experimental model by Castrejon-Pita et al. [11] (left); and the current numerical model structure (right) to simulate performance of a 2 mm fine nozzle diameter (right).

by Castrejon-Pita et al. [11] was examined in more detail. Fig. 2 replicates the 2 mm diameter nozzle inkjet (left), Castrejón-Pita, Morrison [11], with geometry and dimensions of the nozzle and print-head; a model structure of the nozzle is also depicted (right) along with an assumed jet velocity waveform at the print-head inlet. A DOD transient flow operational mode was simulated that employed the same profile as in Castrejon-Pita et al. [11]; such DOD operation is typical to that expected in a piezoelectric push-pull printer. During simulation a no-slip condition was imposed at the wall inside the print-head and a static contact angle on the wall was assumed to be 10^{o} to pin the contact line at the edge of the nozzle outlet [11].

The simulation used 2-D symmetry and computed only the symmetric half of the domain that was divided into three parts, including the ink chamber, the nozzle and the area outside of the nozzle. To achieve a uniform distribution of discretization errors, finer grid sizes were also applied in regions near the nozzle and solid walls, and in the trajectory region of the flight drops where it was expected that derivatives of the variables were critical and could produce large discretization errors. The number of gird cells was chosen to ensure that property differences in adjacent cells were captured during the simulation.

To check the grid size independency, the numerical simulations used three different elements with values of 39,483, 30,916, and 25,378; also, the liquid was a glycerol-water mixture with physical properties of density (1,222 kg/m^3), viscosity (0.1 kg/ms), and surface tension (0.064 N/m). Fig. 3 compares the current simulation results to the published simulation ([11]) and experimental results. For the current study, the best agreement between simulation and experimental data [11], was when the highest (39,483) number of elements was used; the extent of agreement decreased as the number of elements used in the simulation was decreased. Hence, it is concluded that the numerical model could be considered to be governed by the appropriate physics principles and equations and, because of the agreement between the simulation results and experimental data, a grid size of at least 39,483 was necessary before the simulation became independent of the number of elements used.

In Fig. 3, note that the experimental data have a negative or small downward inflow shown outside the print-head inlet boundary. A negative inflow may affect the tail of the liquid thread by pulling

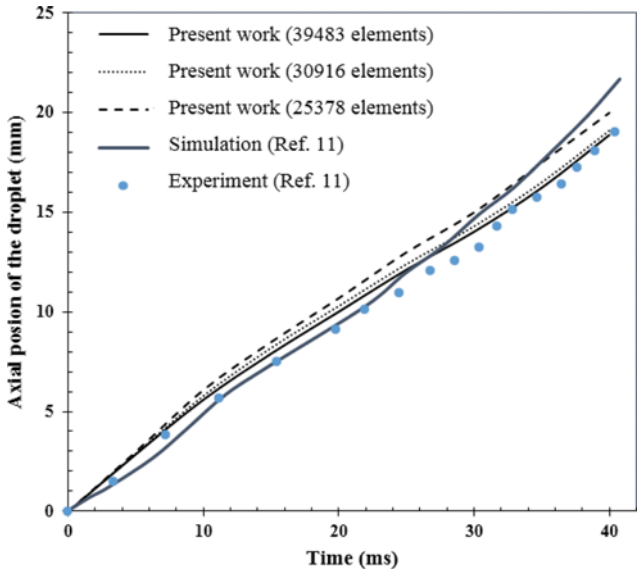

Fig. 3. Our grid independency test validates the current numerical simulation.

the tail toward the nozzle and thus may lead to a decreased forward momentum of tail tip [11]. This negative inflow was neglected in their numerical simulation and resulted in an increased forward momentum value for the droplet after the tail was fully absorbed into the head; consequently, their simulation displayed a slightly overestimated droplet velocity compared to their experimental values. Their model also ignored gravity, which can be expected to counter balance, in some degree, any negative inflow effect. Furthermore, their numerical results were extensively greater than their experimental results in a range between 22-to-40 ms, with increasing departure between the two as the time increased. This trend indicates either the numerical model that was used contained some fundamental miscalculations or an error was associated with an inadequate grid independency test; the latter was not discussed in their article.

Fig. 4 compares droplet shapes from our numerical results and the experimental results [11] at five different times, each separated by 3 ms after liquid filament ejection. The first experimental drop-

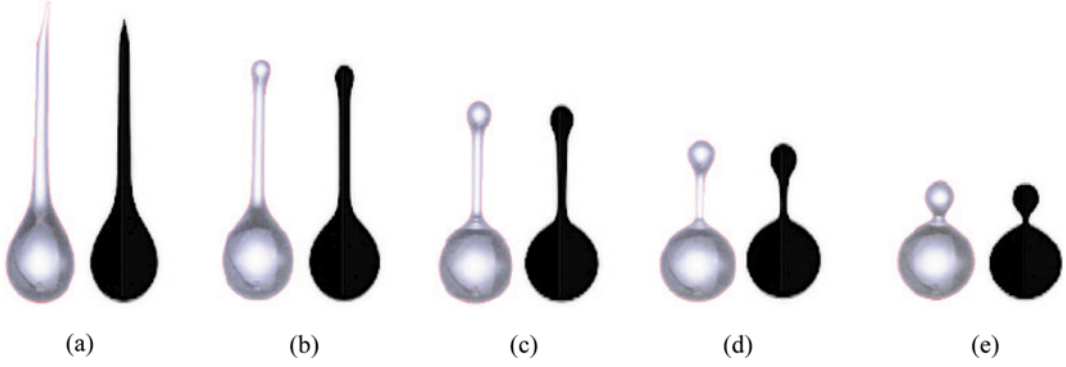

Fig. 4. Five different pairs compare the experimental result of filament evolution ([11]) on the left and our corresponding numerical simulation result on the right. For the experiment, the initiation step (a) was 21 ms after the droplet ejection, while for our numerical simulation it was 20 ms. Each frame (a through e) is separated by 3 ms.

let in Fig. 4(a) was taken at a time=21 ms, while the first simulation droplet was at a time=20 ms. This time difference of 1 ms may be due to a small timing difference associated with experimental uncertainty, could be expected to be difficult to control experimentally, and was the greatest difference between these experimental data and the current simulation results. Nevertheless, all of the droplet images from single-flash photography [11] (displayed on the left side of each part of the figure) were very similar in shape to those from the current simulation (displayed on the corresponding right side of each part of the figure). In contrast to the 1 ms difference between experimental data and current simulation results, the simulation of Castrejón-Pita et al. [11] resulted in a maximum difference of 4 ms between experiment and simulation Hence, the current numerical simulation may be expected to better represent actual droplet qualities.

NUMERICAL METHODS

Liquid jet breakup phenomena can be classified as a multi-phase processes involving liquid and gas flows. The breakup can be described through unsteady-state Navier-Stokes equations in their conservation forms, in which mass and momentum conservation can be written as follows (two dimensional):

$$\frac{\partial \rho}{\partial t}+\nabla\cdot(\rho\vec{V})=0 \tag{1}$$

$$\frac{\partial(\rho\vec{V})}{\partial t}+\nabla\cdot(\rho\vec{V}\vec{V})=-\nabla p+\nabla\cdot[\mu(\nabla\vec{V}+\nabla\vec{V}^{T})]+\rho\vec{g}+\vec{F}_{\sigma} \tag{2}$$

where $\vec{V}$=(u, v), p is the pressure, $\vec{g}$ is the gravitational acceleration, μ is the viscosity, and $\vec{F}_{\sigma}$ is the surface tension force per volume.

In the current study, a VOF model [16,17] is employed to simulate two immiscible phases of air and liquid by solving a single set of momentum equations and tracking the volume fraction of a particular phase in each cell throughout the model domain. Eq. (1) is solved for the volume fraction of one or more phases and to track the interface between them. For a representative phase q, the continuity equation gives us the following:

$$\sum_{q}\frac{1}{\rho_q}\left[\frac{\partial}{\partial t}(\alpha_q\rho_q)+\nabla\cdot(\alpha_q\rho_q\vec{V}_q)\right]=\sum_{q}\frac{1}{\rho_q}\sum_{p=1}^{n}(\dot{m}_{pq}-\dot{m}_{qp}) \tag{3}$$

where $\dot{m}_{pq}$ is the mass transfer from phase p to phase q, and $\dot{m}_{qp}$ is the mass transfer from phase q to phase p. The volume fraction of the primary-phase, which in this study was air, will be obtained based on the following equation:

$$\sum_{q=1}^{n}\alpha_q=1 \tag{4}$$

where α is the volume fraction, and q describes the phases in the system.

Eq. (3) is solved by explicit time discretization as following:

$$\frac{\alpha_q^{n+1}\rho_q^{n+1}-\alpha_q^{n}\rho_q^{n}}{\Delta t}V+\sum_{f}(\alpha_{q,f}^{n}\rho_q\vec{U}_f^{n})=V\left[\sum_{p=1}^{n}(\dot{m}_{pq}-\dot{m}_{qp})\right] \tag{5}$$

where n+1 is the index for the current time step and n is the index for a previous time step, $\alpha_{q,f}$ is phase value of the q^{th} volume fraction computed from a compressive scheme, V is the volume of cell, and U_f is the volume flux through the face, based on normal velocity.

The surface stress tensor due to surface tension is represented as:

$$T=\sigma(I-\hat{n}\otimes\hat{n})|\vec{n}|$$

where I is the unit tensor, σ is the surface tension coefficient, $\otimes$ is the tensor product of two vectors, and

$$\hat{n}=\frac{\vec{n}}{|\vec{n}|}\ \text{ and }\ \vec{n}=\nabla\alpha$$

and the surface tension force is represented as:

$$\vec{F}_{\sigma}=\nabla\cdot T$$

The volume fraction of secondary phase is obtained via Eq. (5) and Eq. (4) can be used to obtain the primarily phase's volume fraction.

In the VOF model, a single momentum equation is solved throughout the domain, and the resulting velocity field is the same at the interphase. The foregoing momentum Eq. (2) is dependent on the volume fraction of the two phases through the properties of ρ and μ; in each control volume, the volume fractions of all phases sum to unity. The fields for all variables and properties are shared by the two phases and are volume-averaged values, if the volume fraction of each of the phases is known at each location. Thus, depending upon the volume fraction values, the physical properties in each cell are purely representative of one of the phases or of a mixture of the phases, and values of properties or desired variables in each cell will be determined based on their respective volume fraction. For instance, if the volume fraction is shown by α, the density in each cell is given by:

$$\rho=\alpha_g\rho_g+(1-\alpha_g)\rho_l \tag{6}$$

where the subscripts g and l represent gas and liquid phases, respectively. Generally, for an n-phase system all of these properties can be represented by:

$$\vartheta=\sum\alpha_q\vartheta_q \tag{7}$$

in which q is a chosen phase and ϑ is a representative property. Hence, the number of equations is 4n+1 equations and the number of unknowns is 5n. Because n−1 additional equations are needed to calculate the unknowns, it is possible to apply constraints on the pressure that all involved phases share the same pressure field, such that:

$$p_q=p,\ \ \forall q\in[1,\ n] \tag{8}$$

The pressure implicit with splitting of operators (PISO) scheme along with two additional corrections, including neighbor correction and skewness correction, were used for the pressure-velocity coupling. Simultaneously, a pressure staggering option scheme and second-order upwind scheme were employed for interpolating the pressure and momentum equations, respectively. Then, a geo-reconstruct scheme was used to reconstruct the interface. Finally, a variable time-stepping method, in which the time step is calculated for a fixed value of the Courant number (0.2), was used for reducing calculation times.

To have a better understanding of the important parameters influencing breakup phenomena, the momentum equation needs to be non-dimensionalized. Considering Eq. (2), and substituting obtained expression for the surface tension force and then nondimensionalizing it based on a length scale (e.g., nozzle radius, R), and a velocity scale (e.g., scaled velocity, U), we can write:

$$\vec{x}^* = \frac{\vec{x}}{R},\ \vec{V}^* = \frac{\vec{V}}{U},\ t^* = \frac{t}{R/U} \text{ and } p^* = \frac{p}{\rho U^2}.$$

$$\frac{U^2}{R}\left[\frac{\partial(\vec{V}^*)}{\partial t^*} + \nabla\cdot(\vec{V}^*\vec{V}^*)\right] = -\frac{U^2}{R}\nabla p^* + \frac{U\mu}{\rho R^2}\nabla\cdot[\nabla\vec{V}^* + \nabla(\vec{V}^*)^T] + \frac{\sigma}{\rho R^2}\nabla\cdot[(I-\hat{n}\otimes\hat{n})|\vec{n}|]$$

So,

$$\frac{\partial(\vec{V}^*)}{\partial t^*} + \nabla\cdot(\vec{V}^*\vec{V}^*) = -\nabla p^* + \frac{1}{Re}\nabla\cdot[\nabla\vec{V}^* + \nabla(\vec{V}^*)^T] + \frac{1}{We}\nabla\cdot[(I-\hat{n}\otimes\hat{n})|\vec{n}|] \quad (9)$$

Eq. (9) shows that by assuming an incompressible flow for a typical inkjet print-head, the breakup phenomenon is controlled by two dimensionless parameters, Re and We numbers.

In general, jet breakup of a liquid filament may arise because of a strangulation of the filament by surface tension which acts as a driving cause, while the inertia and viscous forces act as retarding causes to suppress filament breakup [18]. Accordingly, two independent pi-numbers describing this competitive nature were identified [19] and included We, which can be represented by a ratio of the inertial force-divided by the-surface tension force, and Re, which can be represented by a ratio of the inertia force-divided by the-viscous force. Another pi-number, the Oh number, was derived from a combination of We and Re, where $Oh=We^{1/2}/Re$. Previous research outcomes have discussed these three dimensionless numbers [19], or pi-numbers. For the benefit to past studies, all three pi-numbers are calculated, as following:

$$We = \frac{\rho U^2 R}{\sigma},\ Re = \frac{\rho U R}{\mu} \text{ and } Oh = \frac{\mu}{\sqrt{\rho R \sigma}} \quad (10)$$

where R is the nozzle radius (m), V is the velocity scale of the droplet ejection process (m-s^{-1}) which will be determined later, σ is the surface tension (N-m^{-1}) of liquid drop surrounded by air, and ρ is the density (kg-m^{-3}) of the ejected liquid. Since Oh, We and Re numbers are interdependent, e.g. $Oh=\sqrt{We}/Re$, liquid filament break up may be described while employing either We and Oh, or Re and We, numbers.

Note that recent studies [1,10] have sought to find a boundary between the operating regimes for satellite formation, and have considered two non-dimensional numbers, the aspect ratios l/R', where R' is the radius of the cylindrical filament, and Oh. However, the process of DOD formation is dependent on liquid properties, print-head geometry and the input driving signal [9]. Hence, the current study uses the radius of the nozzle to characterize print-head geometry and the velocity of the droplet as the input driving signal, and enables the following to be stated:

$$l = \text{fn}(\rho, \sigma, \mu, U, R),\ R' = \text{fn}(\rho, \sigma, \mu, U, R) \quad (11)$$

Using a previously discussed scaling analysis technique [19] with two separate characteristic lengths l and R', and using ρ, V and R as the repeating parameters, the following is derived:

$$l/R = \text{fn}(We, Re),\ R'/R = \text{fn}(We, Re)$$

and

$$l/R' = \text{fn}(We, Re) \quad (12)$$

Therefore, the aspect ratio is a function of the two fundamental numbers, We and Re, both of which depend on the liquid properties and nozzle size as well as the droplet velocity. Although the three pi-numbers Oh, Re and We were introduced as a way to characterize the DOD formation process, their interdependency requires to the use of either (Re and We) or (Oh and We) numbers to delineate the boundaries between the two regimes.

RESULTS AND DISCUSSION

Liquid droplet formation processes were studied under a wide range of jetting conditions through an assessment of Oh, We and Re numbers. Fig. 5, which displays the time evolution of the axial tip position for four different values of We and Oh, in which all the curves have an identical slope up to 10 ms. This slope points to the actual ejection speed of the droplet to be 0.6 m/s for all four cases depicted in Fig. 5, as determined by the magnitude of the actuation pulse which gives a velocity scale for characterizing inertial effects. Then, the 0.6 m/s ejection speed was used for calculating the We number.

Fig. 6 shows the simulation results for different jetting conditions, plotted as a function of We and Oh numbers; data are shown for $0.1 \le OH \le 1.0$, a range which is applicable to DOD inkjet printing and typical commercial printers. The solid circles represent the generation of single droplets and the open circles/squares denote the generation of droplets having one/more than one satellite droplets. The boundary between these regimes is shown in the shaded area of Fig. 6, and may be called the transition region; they are regions

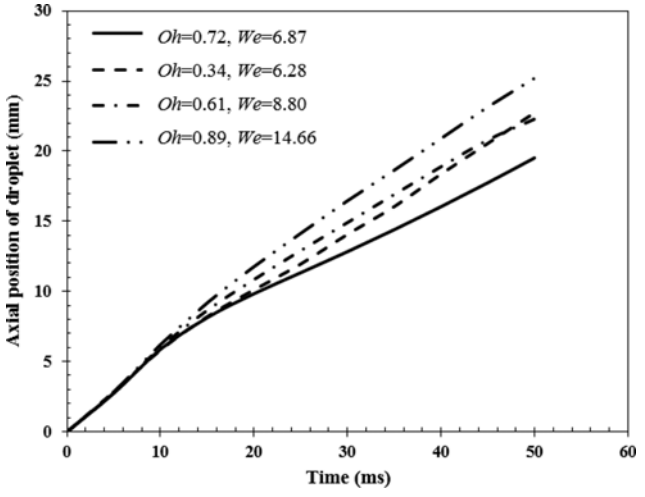

Fig. 5. Axial position of the droplet over time for different Oh and We numbers.

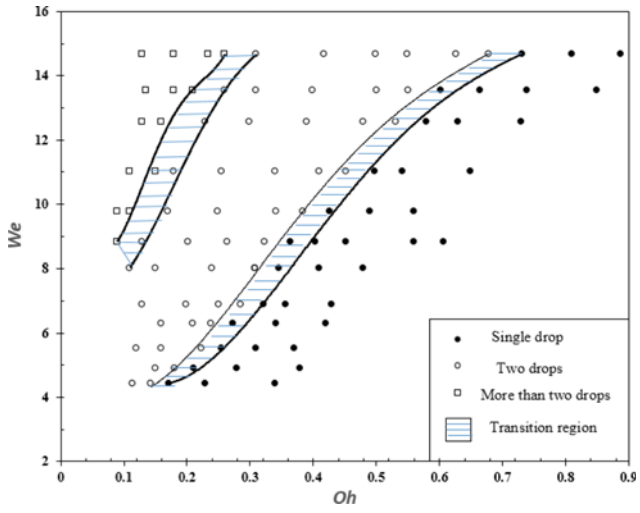

Fig. 6. Criteria for single and multiple break-up based on We and Oh numbers; the solid line represents a distinction line between the two modes.

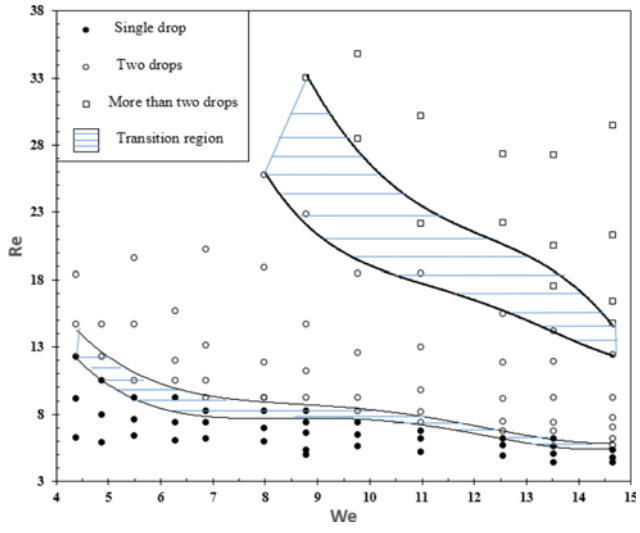

Fig. 7. Criteria for single and multiple break-up based on Re and We numbers.

rather than lines and represent the uncertainties within the precision of the numerical simulation or the errors related to judging whether a specified filament breaks up or not. Outside of the transition regions one can be sure if filaments break up or not.

The information in Fig. 6 shows that at a specified We number an increase in the Oh number is required to transition from breakup producing droplets with satellites to single droplets; in other words, higher fluid viscosities delay liquid ligament breakup and droplet formation. It also suggests that avoiding breakup for a long liquid thread with low surface tension would require an increase in liquid viscosity. The (We and Oh) number plot can be converted to a (Re and We) number plot, as shown in Fig. 7; it also displays transition regions that separate single droplet and droplet with one/more than one satellite regimes.

Experimentally, it is difficult and time-consuming to precisely measure droplet parameters such as initial speed and the initial relative speed of opposite ends of a liquid filament, and the diameter and length of a liquid filament. However, Hoath et al. [1] successfully acquired such data and used it to describe a simple criterion for droplet breakup based on the non-dimensional number Oh and the liquid filament aspect ratio. Their study has important implications but may not be strictly applicable to real ink jet operation because liquid jets that were studied only had small initial relative speeds between their two ends; furthermore, their analyses required very high precision photography to capture the ejected filament physical features, an expensive and time-consuming process.

In contrast, the significance of the current study is to propose and demonstrate a simulation method which provides excellent precision along with close replication of experimental data already available. The results of this simulation demonstrate that specific criteria are required to transition between single and multiple droplet modes as described by either (Oh and We) or (Re and We) couplets, all of which were only dependent on the ejected liquid properties and the velocity waveform at the print-head inlet.

CONCLUSIONS

Present study was dedicated to find a boundary line between the two observed modes of ejected filament from a large-scale ink-jet printer: single and multiple breakup regimes. To reach this goal, a numerical simulation based on the volume-of-fluid model was employed to investigate droplet formation dynamics from a large scale drop-on-demand print-head prototype. Grid independency and comparison with the literature results were done to provide a firm justification, both quantitative and qualitative, for the numerical simulation. This study predicts filament behavior and the transition line between the two regimes with only two effective non-dimensional parameters reflecting competition between driving and retarding forces in terms of combination of either (Oh and We) numbers or (We and Re) numbers. In contrast with the past studies which require experimental data to predict the filament behavior, this study can do the same task only based on the ejected liquid properties and the actuation driving waveform and without experimental measurement data.

ACKNOWLEDGMENTS

Acknowledgment to the institute of research for technology development (IR4TD) for its support.

NOMENCLATURE

Roman Symbols

$\vec{F}_\sigma$: surface tension force [kg/(m^{2}s^2]
$\vec{g}$: gravitational acceleration [ms^2]
I : unit tensor
l : length of cylindrical filament
$\dot{m}_{qp}$: mass transfer from phase q to phase p [kg/s]
$\dot{m}_{pq}$: mass transfer from phase p to phase q [kg/s]
n : index for time step
$\hat{n}$: unit vector of $\vec{n}$

p : pressure [kg/(ms^2)]
R : nozzle radius [m]
R′ : radius of cylindrical filament [m]
t : time [s]
T : surface stress tensor [kg/s^2]
U : scale ejection velocity [m/s]
$\vec{V}$: velocity vector [m/s]
V : volume of the computational cell [m^3]
$\vec{V}^T$: transpose of velocity vector [m/s]
$\vec{x}$: coordinate vector

Greek Symbols

σ : surface tension [kg/s^2]
ρ : density [kg/m^3]
α : volume fraction
μ : viscosity [m^2/s]
ϑ : representative property

REFERENCES

1. S. D. Hoath, S. Jung and I. M. Hutchings, *Physics of Fluids (1994-present)*, **25**, 021701 (2013).
2. R. F. Burr, D. A. Tence, H. P. Le, R. L. Adams and J. C. Mutton, US Patents, 5,495,270 (1996).
3. B. Jo, A. Lee, K. Ahn and S. Lee, *Korean J. Chem. Eng.*, **26**, 339 (2009).
4. A. A. Castrejón-Pita, J. R. Castrejón-Pita and G. D. Martin, *Review of Scientific Instruments*, **83**, 115105 (2012).
5. C. Lee and S. Yi, *Korean J. Chem. Eng.*, **21**, 1153 (2004).
6. A. U. Chen and O. A. Basaran, *Physics of Fluids (1994-present)*, **14**, L1 (2002).
7. O. A. Basaran, *AIChE J.*, **48**, 1842 (2002).
8. D. Im, *Korean J. Chem. Eng.*, **32**, 1 (2015).
9. H. Dong, W. W. Carr and J. F. Morris, *Physics of Fluids (1994-present)*, **18**, 072102 (2006).
10. A. A. Castrejón-Pita, J. R. Castrejón-Pita and I. M. Hutchings, *Physical Review Letters*, **108**, 074506 (2012).
11. J. R. Castrejón-Pita, N. F. Morrison, O. G. Harlen, G. D. Martin and I. M. Hutchings, *Phys. Review E*, **83**, 036306 (2011).
12. J. Fromm, IBM Corp., Yorktown Heights, NY (1981).
13. E. Kim and J. Baek, *Physics of Fluids (1994-present)*, **24**, 082103 (2012).
14. Q. Xu and O. A. Basaran, *Physics of Fluids (1994-present)*, **19**, 102111 (2007).
15. H. Wijshoff, *Physics Reports*, **491**, 77 (2010).
16. F. Yang, S. Zhou, C. Zhang and G. Wang, *Korean J. Chem. Eng.*, **30**, 1843 (2013).
17. S. Poozesh, N. Akafuah and K. Saito. *SAE Technical Paper,* No. 2015-01-0737 (2015).
18. J. M. Delhaye, N. Coutris and L. Herran, *ASME International Mechanical Engineering Congress and Exposition, Proceedings (IMECE)*, **8 C** (2013).
19. R. Emori, K. Saito and K. Sekimoto, *Tokyo, Japan: Gihodo. Second Print in* (2008).